LONGITUDINAL THREE-LABEL SEGMENTATION OF KNEE CARTILAGE

Liang Shan[1], *Cecil Charles*[2], *Marc Niethammer*[1,3]

[1]Department of Computer Science, University of North Carolina at Chapel Hill
[2]Department of Radiology, Duke University,
[3]Biomedical Research Imaging Center, University of North Carolina at Chapel Hill

ABSTRACT

Automatic accurate segmentation methods are needed to assess longitudinal cartilage changes in osteoarthritis (OA). We propose a novel general spatio-temporal three-label segmentation method to encourage segmentation consistency across time in longitudinal image data. The segmentation is formulated as a convex optimization problem which allows for the computation of globally optimal solutions. The longitudinal segmentation is applied within an automatic knee cartilage segmentation pipeline. Experimental results demonstrate that the longitudinal segmentation improves the segmentation consistency in comparison to the temporally-independent segmentation.

Index Terms— longitudinal, three-label, segmentation, cartilage

1. INTRODUCTION

Osteoarthritis (OA) is the most common form of joint disease and a major cause of long-term disability in the US. Since cartilage loss is believed to be the dominating factor in OA, an automatic accurate cartilage segmentation from magnetic resonance (MR) knee images is crucial to study longitudinal cartilage changes for OA based on large image databases.

Several automatic cartilage methods have been proposed recently, e.g., based on a voxel-based classification [1], an active shape model [2], graph-cuts [3], an active appearance model [4], texture analysis [5] and the variation of cartilage thickness [6].

Since subtle changes of cartilage might be indicative of early OA, it is desirable to study the longitudinal cartilage changes from a temporally-consistent segmentation which can mitigate image noise effects. However, the aforementioned methods treat each image volume separately without exploring the temporal consistency within the same subject. For brain segmentation, Xue *et al*. [7] proposed a longitudinal segmentation method by adding a temporal consistency constraint term to a fuzzy clustering segmentation.

The authors thank Pfizer Inc. for providing the data from the Pfizer Longitudinal Study (PLS-A9001140) and gratefully acknowledge support by NIH NIAMS 1R21AR059890-01A1.

We propose a novel general longitudinal three-label segmentation approach and apply it to the cartilage segmentation problem. The longitudinal three-label segmentation is formulated as a convex optimization problem. A temporal consistency term is added to the existing three-label segmentation [8]. We make use of temporally-independent bone and cartilage segmentations to transform the longitudinal image data from native image space to the common longitudinal image space for each subject.

The contributions of this paper include a novel general longitudinal three-label segmentation method, the application of the proposed method to achieve a fully automatic longitudinal cartilage segmentation and the evaluation of longitudinal segmentation on a sizable longitudinal dataset consisting of more than 700 images against temporally-independent segmentation.

The remainder of the paper is organized as follows: Section 2 briefly introduces the existing three-label segmentation method and its application to obtain temporally-independent cartilage segmentation. Section 3 describes the proposed longitudinal three-label segmentation. The transformation from the native image space to the longitudinal image space is explained in section 4. Experimental results are presented in section 5. The paper closes with conclusion and future work.

2. TEMPORALLY-INDEPENDENT THREE-LABEL SEGMENTATION

A three-label segmentation [8] has been proposed to overcome the limitation of the binary segmentation on touching objects. The segmentation energy is formulated by minimizing

$$\begin{aligned} E(u) &= \int_{\mathcal{D}} g\,\|\nabla_{\mathbf{x}} u\| + c\,|\nabla_l u|\ d\mathbf{x}dl, \\ \mathcal{D} &= \Omega \times \mathcal{L},\ u(\mathbf{x},0) = 0,\ u(\mathbf{x},L) = 1. \end{aligned} \tag{1}$$

The energy is defined on an image domain Ω and a labeling space $\mathcal{L} = \{0, ..., L-1\}$; u is a level function whose discontinuity set defines labels; $\nabla_{\mathbf{x}} u$ is the spatial gradient of u, $\nabla_{\mathbf{x}} u = (\partial u/\partial x, \partial u/\partial y, \partial u/\partial z)^T$; $\nabla_l u$ is the gradient in label direction, $\nabla_l u = \partial u/\partial l$; $g > 0$ controls spatial regularization and c defines the labeling cost. This is a convex

formulation and guarantees the separation of the femoral and the tibial cartilage for which a globally optimal solution can be computed.

To obtain temporally-independent cartilage segmentation, the labeling cost c for each label l in $\{\text{FC}, \text{BG}, \text{TC}\}$ ("FC", "BG" and "TC" denote the femoral cartilage, the background and the tibial cartilage respectively) are defined by log-likelihoods for each label:

$$c(\mathbf{x}, l) = -log(p(l|\mathbf{f}(\mathbf{x}))) = -log\left(\frac{p(\mathbf{f}(\mathbf{x})|l) \cdot p(l)}{p(\mathbf{f}(\mathbf{x}))}\right), \quad (2)$$

where $\mathbf{f}(\mathbf{x})$ denotes a *feature* vector at $\mathbf{x}$. The background label "BG" is placed between the femoral cartilage label "FC" and the tibial cartilage label "TC" in order to achieve a symmetric setting.

The local likelihood term $p(\mathbf{f}(\mathbf{x})|l)$ is computed from a probabilistic classification based on the local image appearance [9]. We compute the spatial prior $p(l)$ using propagated labels for femoral and tibial cartilage from multi-atlas registration [9]. The likelihoods and priors are integrated into (2) to solve (1) and we obtain the temporally-independent three-label cartilage segmentation.

3. LONGITUDINAL THREE-LABEL SEGMENTATION

Rather than treating each image separately, we can make use of the temporal consistency of longitudinal image data from the same subject to improve the segmentation. We propose a novel longitudinal three-label segmentation method to mitigate possible noise effect and encourage segmentation consistency across time points. The method is general and capable of solving other segmentation problems with two objects.

Assuming the longitudinal image data for a given subject has been registered into a common space, we formulate the longitudinal three-label segmentation energy as

$$\begin{gathered} E(u) = \int_{\mathcal{D}} g\,\|\nabla_{\mathbf{x}} u\| + c\,|\nabla_l u| + h\,|\nabla_t u|\ d\mathbf{x}dldt, \\ \mathcal{D} = \Omega \times \mathcal{L} \times \mathcal{T},\ u(\mathbf{x}, 0, t) = 0,\ u(\mathbf{x}, L, t) = 1, \end{gathered} \quad (3)$$

where $\mathcal{T}$ is the time domain; $\nabla_t u$ is the gradient in time dimension, $\nabla_t u = \partial u / \partial t$; $h > 0$ controls the temporal regularization. This is a convex formulation and yields a global optimal solution. As the cartilage is a thin structure this energy (defined over a 5-dimensional space) can still be efficiently optimized. Figure 1 demonstrates the benefit of the longitudinal segmentation which is more resistant to image noise than the temporally-independent segmentation.

4. REGISTRATION OF LONGITUDINAL IMAGES

The longitudinal segmentation model (3) requires registered longitudinal data. However the images at different time points are not aligned. Therefore we need to register the longitudinal images of a given subject into a common space (longitudinal space) before performing longitudinal segmentation. Here we use the temporally-independent bone segmentation obtained through a multi-atlas-based approach [9] and the cartilage segmentation discussed in section 2.

Specifically we use independent rigid transformations based on the femur and tibia segmentations to initialize rigid transformations between the temporally-independent femoral and tibial cartilage segmentations (for improved registration robustness). The labeling cost for (3) can then be computed as

$$c(\mathbf{x}, l, t) = -log(p_t(l|\mathbf{f}(\mathbf{x}))) = -log\left(\frac{p_t(\mathbf{f}(\mathbf{x})|l) \cdot p_t(l)}{p_t(\mathbf{f}(\mathbf{x}))}\right), \quad (4)$$

where the subscript t represent the likelihoods at the t-th time point which are propagated from the native image space:

$$\begin{aligned} p_t(\mathbf{f}(\mathbf{x})|\text{FC}) &= R_t^{\text{FC}} \circ R_t^{\text{FB}} \circ p(\mathbf{f}(\mathbf{x})|\text{FC}), \\ p_t(\mathbf{f}(\mathbf{x})|\text{TC}) &= R_t^{\text{TC}} \circ R_t^{\text{TB}} \circ p(\mathbf{f}(\mathbf{x})|\text{TC}), \\ p_t(\text{FC}) &= R_t^{\text{FC}} \circ R_t^{\text{FB}} \circ p(\text{FC}), \\ p_t(\text{TC}) &= R_t^{\text{TC}} \circ R_t^{\text{TB}} \circ p(\text{TC}). \end{aligned} \quad (5)$$

Here, R_t denotes a rigid transform for the t-th timepoint. Superscripts specify the registration ("FC": femoral cartilage, "TC": tibial cartilage, "FB": femoral bone, "TB": tibial bone). The choice of the common space is important. To avoid overlap of femoral and tibial cartilage after registration, we choose the first time-point (baseline image) as the common space because it is expected to have the thickest cartilage. The longitudinal segmentation of each cartilage can then obtained by optimizing (3) with labeling cost defined by (4).

5. EXPERIMENTAL RESULTS

This section compares the proposed longitudinal segmentation against the temporally-independent segmentation on a knee MR image dataset acquired for an OA study. We make use of the Pfizer Longitudinal Dataset (PLS-A9001140) which contains T1-weighted (3D SPGR) images for 155 subjects, imaged at baseline, 3, 6, 12, and 24 months at a resolution of $1.00 \times 0.31 \times 0.31\ mm^3$. Some subjects have missing scans and we have 706 MR images in total. The Kellgren-Lawrence grades (KLG) [10] were determined for all subjects from the baseline scan, classifying 81 as normal control subjects (KLG0), 1 as KLG1 (mild OA), 40 as KLG2 (severe OA) and 33 as KLG3 (server OA).

Expert cartilage segmentations are available for all images in the native image space. The femoral cartilage segmentation is drawn only on the weight-bearing part while the tibial cartilage segmentation covers the entire region. We use images from 18 subjects (13 KLG0s, 2 KLG2s and 3 KLGs) as

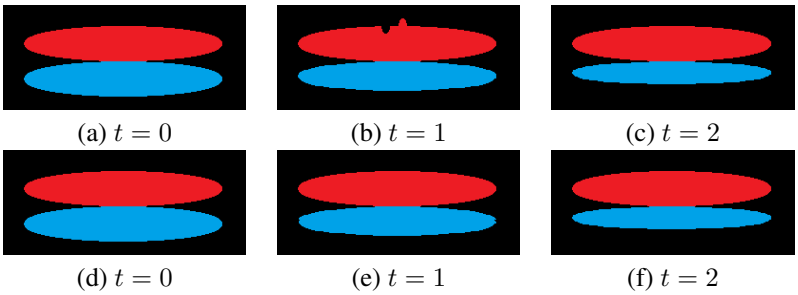

(a) $t = 0$ (b) $t = 1$ (c) $t = 2$

(d) $t = 0$ (e) $t = 1$ (f) $t = 2$

Fig. 1. Synthetic example demonstrating the benefit of longitudinal segmentation. (a), (b) and (c) are longitudinal images and (b) has image noise. (d), (e) and (f) are the corresponding segmentation from the longitudinal segmentation model (3). The segmentation result is resistant to image noise (red object) and still captures the atrophy of the blue object.

training atlases (for multi-atlas registration and local classification) to segment the remaining 137 subjects. Within these 18 subjects, each subject is tested using the other 17 images for training.

Figure 2 compares the mean Dice similarity coefficient (DSC) of the longitudinal segmentation of each cartilage with increasing amount of temporal regularization. The DSCs are computed in both the longitudinal image space and the native image space. The mean DSC increases with an appropriate amount of temporal regularization, which demonstrates the advantage of the longitudinal segmentation model. The difference of the mean DSC in the two spaces is due to the rigid transformations and interpolations.

Table 1 compares the validation statistics in the native image space from the longitudinal segmentation and temporally-independent segmentation. Since we only have one expert segmentation which is drawn timepoint-by-timepoint (and therefore not expected to be longitudinally consistent) we cannot directly assess improvements in segmentation accuracy of the longitudinal method with respect to the individual segmentations. Table 1 indicates that the temporal smoothing inherent in the longitudinal model does not greatly affect the result with respect to *temporally-independent* manual segmentations. However, a more temporally consistent is more biologically plausible, which is achieved by the longitudinal segmentation.

To evaluate the improvement of temporal consistency, we use the weighted sum of number of label changes over time as the temporal consistency measure (TCM) defined by

$$\text{TCM} = \sum_{i=1}^{n-1} \sum_{\mathbf{x} \in \Omega} \frac{|S_{i+1}(\mathbf{x}) - S_i(\mathbf{x})|}{t_{i+1} - t_i}, \qquad (6)$$

where n is number of time points ($n > 1$), $\mathbf{x}$ is a voxel in the image domain Ω, S_i is the segmentation and t_i is the time at i-th time point. The weighting is based on the assumption that label changes are more likely to occur over a longer time period. For those patients who have only one scan available ($n = 1$), the measure is set to 0. We compare the TCM of temporally-independent, longitudinal and expert segmentations of the femoral cartilage for all the subjects in Fig 3. The longitudinal segmentation achieves the best temporal consistency. Note that the expert segmentations are drawn independently in each native image space which explains the high TCM. The same comparison result is also observed for the tibial cartilage.

Table 1. Mean (standard deviation) of DSC, sensitivity and specificity with $g = 0.2$ and $h = 3.0$ computed in the native image space. FC: Femoral cartilage. TC: Tibial cartilage. Lon: Longitudinal segmentation. Ind: Temporally-independent segmentation.

	DSC	Sensitivity	Specificity
Lon-FC	75.0% (4.6%)	78.0% (7.1%)	99.9% (0.04%)
Ind-FC	74.3% (4.8%)	82.2% (7.7%)	99.8% (0.05%)
Lon-TC	80.8% (3.4%)	80.5% (6.2%)	99.8% (0.06%)
Ind-TC	81.8% (3.5%)	84.2% (6.3%)	99.8% (0.07%)

The temporally-independent cartilage segmentation is tested on the cartilage segmentation challenge SKI10 [11] dataset and ranks 5th out of 11 participants. However, the longitudinal cartilage segmentation is not applicable to the SKI10 data because it is not a longitudinal dataset.

6. CONCLUSION AND FUTURE WORK

A novel longitudinal three-label segmentation approach is proposed to encourage the temporal consistency of the segmentation of longitudinal data . The approach is general and can be applied to other longitudinal segmentation problems with two objects. Experimental results on cartilage segmentation demonstrate the improvement in temporal consistency using the proposed longitudinal segmentation against the temporally-independent segmentation.

In the future, we will evaluate the performance of the temporally-independent and the longitudinal segmentations on different stages of OA. We will also perform statistical analysis on cartilage thickness change over time and compare the analysis results from different segmentation methods.

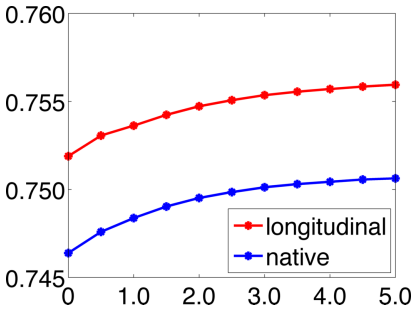

(a) DSC for femoral cartilage

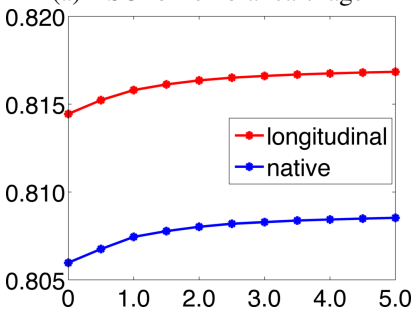

(b) DSC for tibial cartilage

Fig. 2. Change of mean DSC for femoral and tibial cartilage over the amount of temporal regularization h (abscissa). Setting $h = 0$ is equivalent to temporally-independent segmentation in the longitudinal image space. The parameter g is set to be 0.2 for all the tests. The computation of DSC is done in the longitudinal image space (red) by transforming the expert segmentations to the longitudinal image space. The DSCs are also computed in the native image space (blue) by transforming the longitudinal segmentations back into the native image space. Improvement of the mean DSC by including temporal regularization is observed in both spaces. Paired t-tests between two successive settings of h with respect to the mean DSC show statistically significant performance improvement of including temporal regularization for all the four curves with the for a significance level of $\alpha = 0.05$.

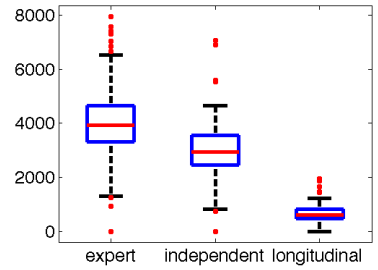

Fig. 3. Boxplots of temporal consistency measure (TCM) of femoral cartilage from expert, temporally-independent ($g = 0.2$) and longitudinal ($g = 0.2$ and $h = 3.0$) segmentations.

7. REFERENCES

[1] J. Folkesson, E. B. Dam, O. F. Olsen, P. C. Pettersen, and C. Christiansen, "Segmenting articular cartilage automatically using a voxel classification approach," *IEEE Transactions on Medical Imaging*, vol. 26, no. 1, pp. 106–115, 2007.

[2] J. Fripp, S. Crozier, S. K. Warfield, and S. Ourselin, "Automatic segmentation and quantitative analysis of the articular cartilages from magnetic resonance images of the knee," *IEEE Transaction on Medical Imaging*, vol. 29, no. 1, pp. 21–27, 2010.

[3] Y. Yin, X. Zhang, R. Williams, X. Wu, D. D. Anderson, and M. Sonka, "Logismos-layered optimal graph image segmentation of multiple objects and surfaces: cartilage segmentation in the knee joint," *IEEE Transaction on Medical Imaging*, vol. 29, no. 12, pp. 2023–2037, 2010.

[4] G. Vincent, C. Wolstenholme, I. Scott, and M. Bowes, "Fully automatic segmentation of the knee joint using active appearance models," *Medical Image Analysis for the Clinic: A Grand Challenge*, pp. 224–230, 2010.

[5] P. Dodin, J. P. Pelletier, J. Martel-Pelletier, and F. Abram, "Automatic human knee cartilage segmentation from 3-D magnetic resonance images," *IEEE Transactions on Biomedical Engineering*, vol. 57, no. 11, pp. 2699–2711, 2010.

[6] H. Seim, D. Kainmueller, H. Lamecker, and M. Bindernagel, "Model-based auto-segmentation of knee bones and cartilage in MRI data," *Medical Image Analysis for the Clinic: A Grand Challenge*, pp. 215–223, 2010.

[7] Z. Xue, D. Shen, and C. Davatzikos, "CLASSIC: Consistent longitudinal alignment and segmentation for serial image computing," *NeuroImage*, vol. 30, pp. 388–399, 2006.

[8] L. Shan, C. Zach, and M. Niethammer, "Automatic three-label bone segmentation from knee MR images," *IEEE International Symposium on Biomedical Imaging*, pp. 1325–1328, 2010.

[9] L. Shan, C. Charles, and M. Niethammer, "Automatic multi-atlas-based cartilage segmentation from knee MR images," *IEEE International Sysmposium on Biomedical Imaging*, pp. 1028–1031, 2012.

[10] J. Kellgren and J. Lawrence, "Radiological assessment of osteoarthritis," *Annals of Rheumatic Diseases*, vol. 16, no. 4, pp. 494–502, 1957.

[11] T. Heimann, B.J. Morrison, M.A. Styner, M. Niethammer, and S.K. Warfield, "Segmentation of knee images: a grand challenge," *Proc. MICCAI Workshop on Medical Image Analysis for the Clinic*, pp. 207–214, 2010.